

Xuemin Wang¹

Mem. ASME

Department of Mechanical Engineering,
Georgia Southern University,
Statesboro, GA 30458
e-mail: xueminwang@georgiasouthern.edu

Tingge Xu

Mem. ASME

Department of Mechanical Engineering,
The University of Texas at Dallas,
Richardson, TX 75080
e-mail: Tingge.Xu@utdallas.edu

Rui Zhang

Mem. ASME

Department of Mechanical Engineering,
The University of Texas at Dallas,
Richardson, TX 75080
e-mail: rui.zhang@utdallas.edu

Monica Jung de Andrade

Alan G. MacDiarmid NanoTech Institute,
The University of Texas at Dallas,
Richardson, TX 75080
e-mail: monica.jung@utdallas.edu

Pruthul Kokkada

Mem. ASME

Department of Aerospace Engineering & Mechanics,
The University of Alabama,
Tuscaloosa, AL 35487
e-mail: pkokkadar@crimson.ua.edu

Dong Qian

Mem. ASME

Department of Mechanical Engineering,
The University of Texas at Dallas,
Richardson, TX 75080
e-mail: Dong.Qian@utdallas.edu

Samit Roy

Fellow ASME

Department of Aerospace Engineering & Mechanics,
The University of Alabama,
Tuscaloosa, AL 35487
e-mail: sroy@eng.ua.edu

Ray H. Baughman

Alan G. MacDiarmid NanoTech Institute,
The University of Texas at Dallas,
Richardson, TX 75080
e-mail: ray.baughman@utdallas.edu

Hongbing Lu¹

Fellow ASME

Department of Mechanical Engineering,
The University of Texas at Dallas,
Richardson, TX 75080
e-mail: hongbing.lu@utdallas.edu

Modeling the Compressive Buckling Strain as a Function of the Nanocomposite Interphase Thickness in a Carbon Nanotube Sheet Wrapped Carbon Fiber Composite

Polymer matrix composites have high strengths in tension. However, their compressive strengths are much lower than their tensile strengths due to their weak fiber/matrix interfacial shear strengths. We recently developed a new approach to fabricate composites by overwrapping individual carbon fibers or fiber tows with a carbon nanotube sheet and subsequently impregnate them into a matrix to enhance the interfacial shear strengths without degrading the tensile strengths of the carbon fibers. In this study, a theoretical analysis is conducted to identify the appropriate thickness of the nanocomposite interphase region formed by carbon nanotubes embedded in a matrix. Fibers are modeled as an anisotropic elastic material, and the nanocomposite interphase region and the matrix are considered as isotropic. A microbuckling problem is solved for the unidirectional composite under compression. The analytical solution is compared with finite element simulations for verification. It is determined that the critical load at the onset of buckling is lower in an anisotropic carbon fiber composite than in an isotropic fiber composite due to lower transverse properties in the fibers. An optimal thickness for nanocomposite interphase region is determined, and this finding provides a guidance for the manufacture of composites using aligned carbon nanotubes as fillers in the nanocomposite interphase region.

[DOI: 10.1115/1.4044086]

¹Corresponding authors.

Contributed by the Applied Mechanics Division of ASME for publication in the JOURNAL OF APPLIED MECHANICS. Manuscript received March 25, 2019; final manuscript received June 12, 2019; published online July 18, 2019. Assoc. Editor: Yashashree Kulkarni.

1 Introduction

Low-density, high-strength composite materials play a critical role in a wide range of areas including aerospace, defense, sports, transportation, and renewable energy. Composites provide improved energy efficiency, easier mobility, agility, and desirable aesthetics. The high-tensile strengths in composites are derived from fibers impregnated in the polymer matrix. Carbon fibers are one of the most widely used fibers due to their high strengths, electrical conductivity, corrosion resistance, and high thermal conductivity. Carbon fiber composites are used in actuators [1,2], structural materials [3], and large airliners [4,5]. However, the compressive strengths of composites are in general much lower than their corresponding tensile strengths due to the fact that under compression, the fibers tend to fail in fiber microbuckling (or kinking) before compressive fracture occurs [6–15]. An analytical model to calculate the compressive strength was first proposed by Rosen [16] for unidirectional composites. Subsequently, other models were developed to determine the compressive strengths of composites. Based on the Rosen work, a 3D analysis was conducted, and the numerical results were consistent with the experimental data for aluminum and steel-reinforced epoxy but not for graphite/epoxy and boron/epoxy [17]. Unknown boundary conditions of the microbuckling region and initial misalignment were also taken into account by introducing factors in the Rosen model [18,19]. Fiber-matrix bond condition and matrix slippage were considered in the model [20] where a fiber was assumed as a beam resting on an elastic foundation. Theory of elasticity was used to solve the microbuckling problem and finite element analysis (FEA) was carried out to verify closed-form solution [21]. Some recent papers analyzed further the fiber microbuckling problems [22–27]. In analysis, the fibers are usually considered as isotropic. In practice, however, fibers are in general transversely isotropic [28–30], determined by Raman spectroscopy, nanoindentation, and micromechanics methods. In addition, fiber misalignment and matrix yield are known to influence compressive strengths in unidirectional composites [31,32].

In order to study properly the compressive strengths of composites, researchers focused on investigating the fiber/matrix interface. A finite interphase region was assumed to exist between a fiber and the matrix [33–36]. The published theoretical work considered usually an interface rather than an interphase region, which is a layer of material between carbon fiber and matrix that could have mechanical properties different from the matrix. Recently, it was determined that by enforcing the interphase region, compressive strengths can be improved [37]. The grafting of carbon nanotubes (CNTs) onto the surface of the carbon fibers through chemical vapor deposition can improve the interfacial shear strength (IFSS), resulting in interfacial shear strength 150% higher than that of the composite without CNTs. However, this technique usually leads to a degradation of carbon fiber in-plane properties due to the chemical processing of the carbon fibers.

As an alternative approach, a novel method was introduced in which a carbon fiber was wrapped by CNT sheet and then impregnated into a polymer matrix, producing a nanocomposite layer in the interphase region [38]. In this work, the compressive buckling of a unidirectional polymer matrix composite containing a CNT polymer nanocomposite interphase region is investigated. In the study, the fiber is considered as anisotropic, and the interphase region and the matrix are considered as isotropic. The results obtained by modeling fiber as anisotropic are compared with an otherwise isotropic fiber. We also investigate the effect of mechanical properties and thickness of the interphase region on the compressive strength. FEA simulations are carried out to compare with the theoretical results and study the effect of nanocomposite interphase on the compressive strengths when the fiber volume fraction is high. The approach is for the general case where there is an interphase layer between fiber and matrix, with CNT nanocomposite interphase layer being a special case of the interphase. The model

works for some of the other interphase layers including nanoclay or graphene modified interphase.

2 Theoretical Analysis

We describe first the method for preparation of a CNT sheet wrapped carbon fiber composite. In this process, at first, a CNT forest is grown on a substrate. Next, the CNTs are pulled out using a knife edge to allow CNT heads to bind to tails to form a sheet. The CNT sheet drawn from the CNT forest is a mesoporous aerogel with high-specific surface area [39], consequently a small amount of CNT sheet by weight can be used to wrap around a large volume of carbon fibers [38]. Figure 1 shows a self-supporting long CNT sheet drawn from a carbon nanotube forest. The CNT sheet is then used to wrap a carbon fiber. Figure 2(a) shows a schematic diagram of a carbon fiber being wrapped around circumferentially by a carbon nanotube sheet at a wrapping bias angle α . The CNT wrapped carbon fiber is then embedded into a polymer matrix. The inner ply of the CNT sheet adheres to the carbon fiber via the van der Waals force. Figure 2(b) shows an SEM micrograph for a single carbon fiber. The bias angles used to wrap CNT sheet around a carbon fiber are 30 deg and 45 deg in Figs. 2(c) and 2(d), respectively. Then, the CNT sheet wrapped carbon fiber is embedded into a polymer matrix, forming a nanocomposite of CNT sheet and epoxy at the interphase region. Figures 3(a) and 3(b) show the surface topography observed by atomic force microscopy of a carbon fiber, and a CNT sheet scrolled carbon fiber embedded in a polymer matrix separately.

Modulus measurement [40–42] was made using a cube corner nanoindenter tip from the carbon fiber and outward to the nanocomposite and polymer with indents shown in Fig. 4(a). The modulus increased from 3.1 GPa (neat polymer) to 24.7 GPa(nanocomposite) for the CNT sheet wrapped carbon fiber at a bias angle 0 deg, and 13.2 GPa for CNT sheet wrapped carbon fiber at a bias angle 45 deg as shown in Fig. 4(b).

Based on these experiments, a theoretical model was established to analyze the compressive buckling in order to optimize the thickness of the nanocomposite interphase. The composite consists of three regions occupied by fiber, nanocomposite (interphase region), and matrix. Figure 5 shows a schematic diagram of the three regions in a CNT wrapped carbon fiber composite. The fiber is modeled as transversely isotropic, and the nanocomposite and the matrix (e.g., epoxy) are modeled as an isotropic, linearly elastic continuum, respectively. If the volume fraction of the fibers is low and the fibers are dilute in the polymer matrix, the problem can be simplified to a single fiber wrapped with CNT sheet impregnated in an infinite matrix. A schematic diagram is shown in Fig. 5. It is assumed that the binding at the fiber/interphase region and the interphase region/matrix interface is perfect so that displacement and stress are continuous at the interface. The composite is subjected to a plane strain deformation in the x - y plane. Subscripts 1, 2, and 3 represent the fiber, interphase region, and matrix, respectively. The entire composite laminate is assumed to be compressed in the fiber direction by a rigid platen.

From the uniformly strained state to the perturbed state, two deformation modes of are possible for the fiber. In this work, as the fiber modulus is significantly higher than that of matrix, an

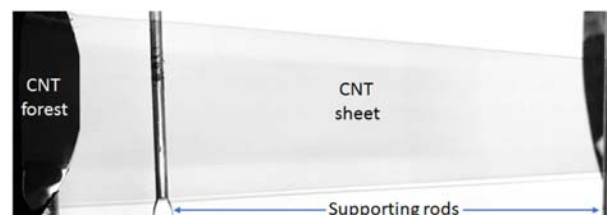


Fig. 1 Photograph of a CNT sheet drawn from a CNT forest

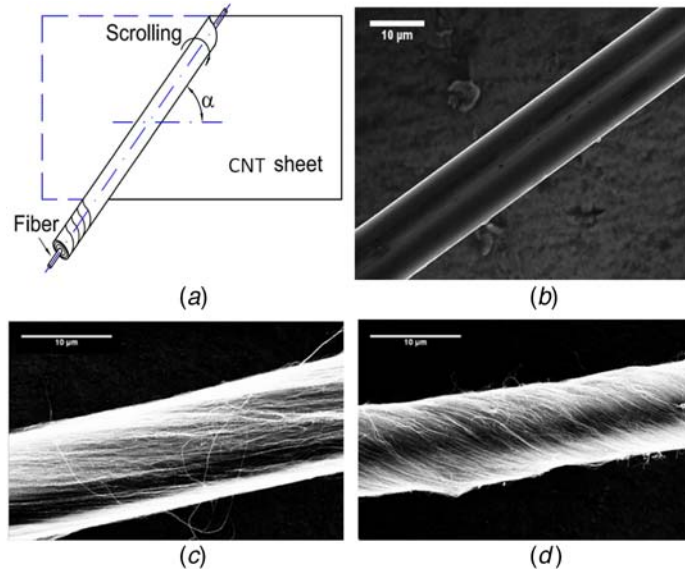


Fig. 2 CNT sheet wrapping a single carbon fiber: (a) a schematic diagram showing a CNT scrolling a carbon fiber, (b) SEM images of the single carbon fiber, (c) SEM micrograph showing a segment of the single carbon fiber with $\alpha = 30$ deg wrapping bias angle, and (d) SEM micrograph showing segment of the single carbon fiber with $\alpha = 45$ deg wrapping bias angle (Courtesy: University of Texas-Dallas).

antisymmetric mode prevails, as identified in the previous studies [15,43]. The fiber displacements under the perturbation should satisfy the antisymmetric conditions.

$$\begin{aligned} u_1(x_1, y_1) &= -u_1(x_1, y_1) \\ v_1(x_1, y_1) &= v_1(x_1, -y_1) \end{aligned} \quad (1)$$

At first, when an aligned fiber/CNTs-reinforced composite is subjected to uniaxially applied uniform strain, the corresponding stress in dimensionless form for the interphase region and the matrix is

given by $s_i = \sigma/2G_i$ ($i = 2, 3$), where σ_{x_i} is the stress in the x_i direction and G_i is the shear modulus. Note that $i = 1$ for the fiber, $i = 2$ for the matrix/CNT interphase region, and $i = 3$ for the matrix. When the fiber is assumed to be transversely isotropic, the number of independent material constants reduces to five; they are E_{fx_1} , E_{fy_1} , $G_{x_1y_1}$, $\nu_{x_1y_1}$ and $\nu_{y_1z_1}$. Equilibrium equations for the solid with a small perturbation are well documented [43]. Neglecting body forces, the equilibrium equations governing the incremental stresses due to the perturbation are

$$\begin{aligned} \frac{\partial(\sigma_x - \omega_z \sigma_{xy}^0 + \omega_y \sigma_{xz}^0)}{\partial x} + \frac{\partial(\sigma_{xy} - \omega_z \sigma_y^0 + \omega_y \sigma_{yz}^0)}{\partial y} + \frac{\partial(\sigma_{xz} - \omega_z \sigma_{yz}^0 + \omega_y \sigma_z^0)}{\partial z} &= 0 \\ \frac{\partial(\sigma_{xy} - \omega_x \sigma_{xz}^0 + \omega_z \sigma_x^0)}{\partial x} + \frac{\partial(\sigma_y - \omega_x \sigma_{yz}^0 + \omega_z \sigma_{xy}^0)}{\partial y} + \frac{\partial(\sigma_{yz} - \omega_x \sigma_z^0 + \omega_z \sigma_{xz}^0)}{\partial z} &= 0 \\ \frac{\partial(\sigma_{xz} - \omega_y \sigma_x^0 + \omega_x \sigma_{xy}^0)}{\partial x} + \frac{\partial(\sigma_{yz} - \omega_y \sigma_{xy}^0 + \omega_x \sigma_y^0)}{\partial y} + \frac{\partial(\sigma_z - \omega_y \sigma_{xz}^0 + \omega_x \sigma_{yz}^0)}{\partial z} &= 0 \end{aligned} \quad (2)$$

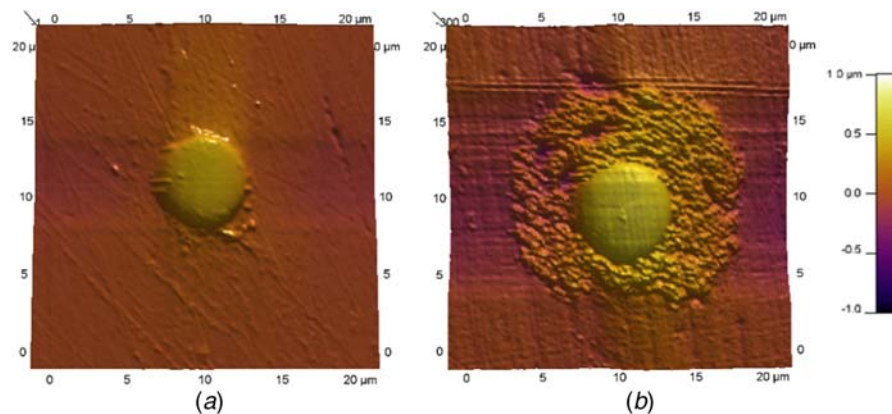
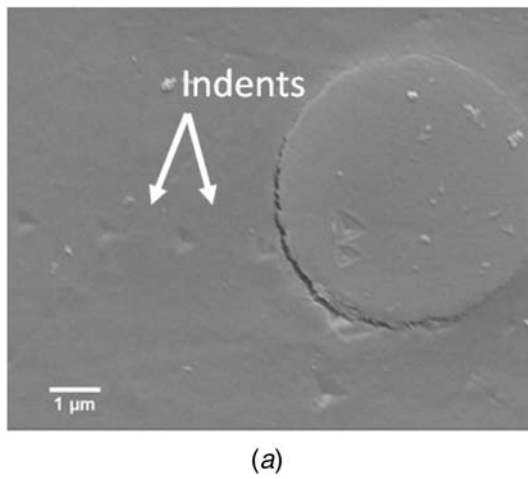


Fig. 3 Surface topographs taken by atomic force microscopy: (a) a single carbon fiber and (b) CNT scrolled single carbon fiber when embedded in polymer matrix after polishing (Courtesy: University of Texas-Dallas).



(a)

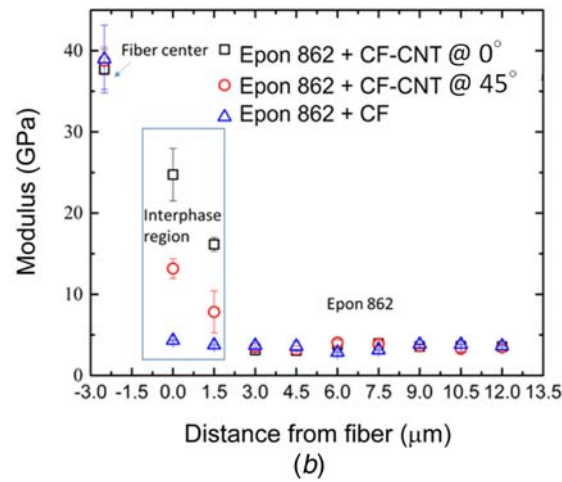


Fig. 4 (a) SEM images indents of composite with CNT at bias angle 0 deg and (b) Young's modulus of the nano-composite and the matrix [47]. Note that the measured fiber modulus is lower than the actual value as the fiber anisotropy, and the compliant matrix are not considered in the nanoindentation measurement. (Courtesy: University of Texas-Dallas).

In Eq. (2), the superscript “0” indicates the unbuckled state and the symbols without superscript represent the perturbed state. Note that $\omega_z = (1/2)(\partial u/\partial y - \partial v/\partial x)$, $\omega_x = \omega_y = 0$, in a plane strain problem, where u and v are independent of z and ω is zero. With the nonzero component $\sigma_x^0 = -\sigma_x$, the above equations are simplified to the following equations:

$$\begin{aligned} \frac{\partial \sigma_x}{\partial x} + \frac{\partial \sigma_{xy}}{\partial y} + \frac{\partial \sigma_{xz}}{\partial z} &= 0 \\ \frac{\partial(\sigma_{xy} - \omega_z \sigma_x)}{\partial x} + \frac{\partial \sigma_y}{\partial y} + \frac{\partial \sigma_{yz}}{\partial z} &= 0 \\ \frac{\partial \sigma_{xz}}{\partial x} + \frac{\partial \sigma_{yz}}{\partial y} + \frac{\partial \sigma_z}{\partial z} &= 0 \end{aligned} \quad (3)$$

In the next step, Eq. (3) and the strain displacement relationships $\epsilon_x = \partial u/\partial x$, $\epsilon_y = \partial v/\partial y$, and $\epsilon_{xy} = (1/2)(\partial v/\partial x + \partial u/\partial y)$ are applied to the fiber, interphase region, and matrix individually.

2.1 Governing Equations for the Carbon Fiber. The fiber is considered as a homogeneous, linearly elastic, and transversely

isotropic solid. The nanocomposite interphase region and the matrix are considered as homogeneous and linearly isotropic. The constitutive equations for the transversely isotropic fiber are given by

$$\begin{bmatrix} \sigma_{x_1} \\ \sigma_{y_1} \\ \sigma_{z_1} \end{bmatrix} = \begin{bmatrix} \frac{(-v_{y_1 z_1}^2 + 1)E_{f_1}}{\Delta} & \phi & 0 \\ \phi & \frac{(1 - v_{y_1 x_1} v_{x_1 y_1})E_{f_1}}{\Delta} & 0 \\ 0 & 0 & 2G_{x_1 y_1} \end{bmatrix} \begin{bmatrix} \epsilon_{x_1} \\ \epsilon_{y_1} \\ \epsilon_{z_1} \end{bmatrix} \quad (4)$$

where Δ and ϕ are given as

$$\begin{aligned} \Delta &= (v_{y_1 z_1} + 1)(1 - v_{y_1 z_1} - 2v_{y_1 x_1} v_{x_1 y_1}) \\ \phi &= \frac{(1 + v_{y_1 z_1})v_{y_1 x_1} E_{f_1}}{\Delta} \end{aligned} \quad (5)$$

Equation (4) and the strain displacement relationships are then substituted into Eq. (3), yielding the following equations:

$$\begin{aligned} \frac{(1 - v_{y_1 z_1}^2)E_{f_1}}{\Delta} \frac{\partial^2 u_1}{\partial x_1^2} + G_{x_1 y_1} \frac{\partial^2 u_1}{\partial y_1^2} + (G_{x_1 y_1} + \phi) \frac{\partial^2 v_1}{\partial x_1 y_1} &= 0 \\ \left(G_{x_1 y_1} - \frac{\sigma_{x_1}}{2}\right) \frac{\partial^2 v_1}{\partial x_1^2} + \frac{(1 - v_{y_1 x_1} v_{x_1 y_1})E_{f_1}}{\Delta} \frac{\partial^2 v_1}{\partial y_1^2} &= 0 \end{aligned} \quad (6)$$

Displacements of the fiber are antisymmetric about x_1 , and therefore, Eq. (6) has a solution in the following form:

$$\begin{aligned} u_1(x_1, y_1) &= f(y_1) \sin(\alpha x_1) \\ v_1(x_1, y_1) &= g(y_1) \cos(\alpha x_1) \end{aligned} \quad (7)$$

where $\alpha = 2/\lambda_w$ and λ_w is the buckle wavelength. Then, substituting Eq. (7) into Eq. (6) and eliminating $g(y_1)$ yield the following equation for $f(y_1)$:

$$a_1 \frac{\partial^4 f(y_1)}{\partial y_1^4} + a_2 \alpha^2 \frac{\partial^2 f(y_1)}{\partial y_1^2} + a_3 \alpha^4 f(y_1) = 0 \quad (8)$$

Similarly, eliminating $f(y_1)$ gives an equation for $g(y_1)$.

$$a_1 \frac{\partial^4 g(y_1)}{\partial y_1^4} + a_2 \alpha^2 \frac{\partial^2 g(y_1)}{\partial y_1^2} + a_3 \alpha^4 g(y_1) = 0 \quad (9)$$

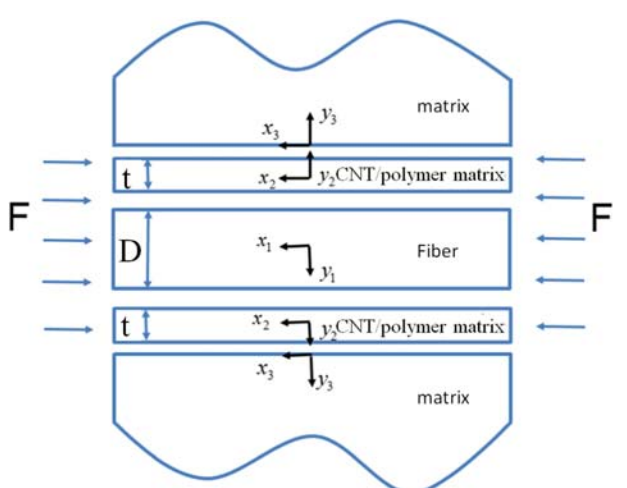


Fig. 5 Configuration of a composite under unidirectional compression in the fiber direction

where a_1 , a_2 , and a_3 are constants given as

$$\begin{aligned} a_1 &= -G_{x_1 y_1} \frac{(1 - v_{y_1 x_1} v_{x_1 y_1}) E_{f_{x_1}}}{\Delta} \\ a_2 &= \frac{(1 - v_{y_1 x_1} v_{x_1 y_1})(1 - v_{y_1 z_1}^2) E_{f_{x_1}} E_{f_{y_1}}}{\Delta^2} - G_{x_1 y_1} \sigma_{x_1} - \frac{\sigma_{x_1}}{2} \phi - 2G_{x_1 y_1} \phi - \phi^2 \\ a_3 &= \frac{(-1 + v_{y_1 z_1}^2) E_{f_{x_1}}}{\Delta} \left(-\frac{\sigma_{x_1}}{2} + G_{x_1 y_1} \right) \end{aligned} \quad (10)$$

The solutions to Eqs. (8) and (9) are

$$\begin{aligned} u_1(x_1, y_1) &= (-B_1 + k_1 D_1) \sinh(\beta_1 \alpha y_1) \sin(\alpha x_1) \\ v_1(x_1, y_1) &= (B_1 m_1 + D_1) \cosh(\beta_1 \alpha y_1) \cos(\alpha x_1) \end{aligned} \quad (11)$$

where $\beta_1 = \sqrt{-a_2/2a_1 + \sqrt{a_2^2 - 4a_1 a_3}}$ and k_1 and m_1 are calculated by the following equations:

$$\begin{aligned} m_1 &= \left(\frac{(1 - v_{y_1 z_1}^2) E_{f_{x_1}}}{\Delta} - G_{x_1 y_1} \beta_1^2 \right) / ((G_{x_1 y_1} + \phi) \beta_1) \\ k_1 &= (G_{x_1 y_1} + \phi) \beta_1 / \left(-\frac{(1 - v_{y_1 z_1}^2) E_{f_{x_1}}}{\Delta} + G_{x_1 y_1} \beta_1^2 \right) \end{aligned} \quad (12)$$

2.2 Governing Equations for the Interphase Region and the Matrix.

The generalized Hook's law for the linearly isotropic interphase region and matrix takes the following form:

$$\sigma_{mn} = \lambda \delta_{mn} \epsilon_{kk} + 2G e_{mn} \quad (13)$$

where m , n , and k are indices representing x_2 , y_2 , and z_2 and x_3 , y_3 , and z_3 , λ is the Lamé constant, G is the shear modulus. Substitution of Eq. (13) into Eq. (3) yields the following equations:

$$\begin{aligned} (\lambda_i + 2G_i) \frac{\partial^2 u_i}{\partial x_i^2} + G_i \frac{\partial^2 u_i}{\partial y_i^2} + (\lambda_i + G_i) \frac{\partial^2 v_i}{\partial x_i y_i} &= 0 \\ (\lambda_i + 2G_i) \frac{\partial^2 v_i}{\partial y_i^2} + \left(G_i - \frac{\sigma_{x_i}}{2} \right) \frac{\partial^2 v_i}{\partial x_i^2} + \left(\lambda_i + G_i + \frac{\sigma_{x_i}}{2} \right) \frac{\partial^2 v_i}{\partial x_i y_i} &= 0 \end{aligned} \quad (14)$$

In Eq. (14), the index i takes the values of 2 or 3; 2 indicates the interphase region while 3 represents the matrix. A similar method is used to solve Eq. (14), and the displacement fields for the interphase region and the matrix are obtained. In the interphase region, the solution is given as

$$\begin{aligned} u_2(x_2, y_2) &= [-B_2 \sinh(\alpha y_2) - A_2 \cosh(\alpha y_2) \\ &\quad + k_2 D_2 \sinh(\mu_2 \alpha y_2) + k_2 C_2 \cosh(\mu_2 \alpha y_2)] \sin(\alpha x_2) \\ v_2(x_2, y_2) &= [A_2 \sinh(\alpha y_2) + B_2 \cosh(\alpha y_2) \\ &\quad + C_2 \sinh(\mu_2 \alpha y_2) + D_2 \cosh(\mu_2 \alpha y_2)] \cos(\alpha x_2) \end{aligned} \quad (15)$$

where $k_2 = \mu_2(\beta_2 + 0.5)/0.5\mu_2^2 - \beta_2 - 1$, $\beta_2 = \lambda_2/2G_2$ and $\mu_2 = \sqrt{1 - s_2^2}$.

For the matrix, the solution is given by

$$\begin{aligned} u_3(x_3, y_3) &= [B_3 e^{-\alpha y_3} - k_3 D_3 e^{-\mu_3 \alpha y_3}] \sin(\alpha x_3) \\ v_3(x_3, y_3) &= [B_3 e^{-\alpha y_3} + D_3 e^{-\mu_3 \alpha y_3}] \cos(\alpha x_3) \end{aligned} \quad (16)$$

where $k_3 = \mu_3(\beta_3 + 0.5)/0.5\mu_3^2 - \beta_3 - 1$, $\beta_3 = \lambda_3/2G_3$ and $\mu_3 = \sqrt{1 - s_3^2}$, and B_i , D_i ($i = 1, 2, 3$) and A_2 , C_2 are eight unknown constants.

2.3 Application of Boundary Conditions. The force boundary conditions for Eq. (3) are given below:

$$\begin{aligned} \Delta f_x &= (\sigma_x - \omega_z \sigma_{xy}^\circ + \omega_y \sigma_{xz}^\circ) \kappa + (\sigma_{xy} - \omega_z \sigma_{yz}^\circ + \omega_y \sigma_{xy}^\circ) \theta \\ &\quad + (\sigma_{xz} - \omega_z \sigma_{yz}^\circ + \omega_y \sigma_{xz}^\circ) \mu \\ \Delta f_y &= (\sigma_{xy} - \omega_x \sigma_{xz}^\circ + \omega_z \sigma_x^\circ) \kappa + (\sigma_y - \omega_x \sigma_{yz}^\circ + \omega_z \sigma_{xy}^\circ) \theta \\ &\quad + (\sigma_{yz} - \omega_x \sigma_z^\circ + \omega_z \sigma_{xz}^\circ) \mu \\ \Delta f_z &= (\sigma_{xz} - \omega_y \sigma_x^\circ + \omega_x \sigma_{xy}^\circ) \kappa + (\sigma_{yz} - \omega_y \sigma_{xy}^\circ + \omega_x \sigma_y^\circ) \theta \\ &\quad + (\sigma_z - \omega_y \sigma_{xz}^\circ + \omega_x \sigma_{yz}^\circ) \mu \end{aligned} \quad (17)$$

The displacements and traction vectors are assumed to be continuous at the fiber/interphase region and interphase region/matrix boundary, and the continuity conditions are given as below. At the interface between carbon fiber and interphase region, where $y_1 = D/2$, $y_2 = -t/2$ as shown in Fig. 5,

$$\begin{aligned} u_1 - u_2 &= 0 \\ v_1 - v_2 &= 0 \\ \Delta f_{x_1} - \Delta f_{x_2} &= 0 \\ \Delta f_{y_1} - \Delta f_{y_2} &= 0 \end{aligned} \quad (18)$$

At the interface between the CNT/matrix nanocomposite interphase region and the neat resin, that is, at $y_2 = t/2$ and $y_3 = 0$ in Fig. 5,

$$\begin{aligned} u_2 - u_3 &= 0 \\ v_2 - v_3 &= 0 \\ \Delta f_{x_2} - \Delta f_{x_3} &= 0 \\ \Delta f_{y_2} - \Delta f_{y_3} &= 0 \end{aligned} \quad (19)$$

The displacement fields provided in Eqs. (11), (15), and (16) and traction Eq. (17) are substituted into Eqs. (18) and (19) to obtain eight linear algebraic homogeneous equations, which are used to determine the eight unknown constants B_i , D_i ($i = 1, 2, 3$) and A_2 , C_2 . The determinant of the matrix M should be zero for nontrivial solutions. Once the critical stress and its corresponding buckling wavelength are found, the eight constants can be determined up to an arbitrary constant. The matrix M is

$$M = \begin{bmatrix} -n_1 & -n_2 & 0 & k_1 n_1 & k_2 n_3 & 0 & c_2 & -k_2 c_3 \\ -m_1 c_1 & -c_2 & 0 & c_1 & -c_3 & 0 & n_2 & n_3 \\ t_1 c_1 & 2G_2 c_2 & 0 & t_2 c_1 & t_5 c_3 & 0 & -2G_2 n_2 & -t_5 n_3 \\ t_3 n_1 & 2G_2 n_2 & 0 & t_4 n_4 & t_6 n_3 & 0 & -2G_2 c_2 & -t_6 c_3 \\ 0 & -n_2 & -1 & 0 & k_2 n_3 & k_3 & -c_2 & k_2 c_3 \\ 0 & c_2 & -1 & 0 & c_3 & -1 & n_2 & n_3 \\ 0 & -2G_2 c_2 & 2G_3 & 0 & -t_5 c_3 & t_8 & -2G_2 n_2 & -t_5 n_3 \\ 0 & 2G_2 n_2 & 2G_3 & 0 & t_6 n_3 & t_6 & 2G_2 c_2 & t_6 c_3 \end{bmatrix} \quad (20)$$

where n_i ($i = 1, 2, 3, 4$) and t_j ($j = 1, 2, 3, \dots, 8$) are defined as follows:

$$\begin{aligned} n_1 &= \sinh(\beta_1 h_1), & c_1 &= \cosh(\beta_1 h_1) \\ n_2 &= \sinh(h_2), & c_2 &= \cosh(h_2) \\ n_3 &= \sinh(\mu_2 h_2), & c_3 &= \cosh(\mu_2 h_2) \\ n_4 &= \sinh(\mu_1 h_1), & t_1 &= G_{12}(-m_1 - \beta_1) \\ t_2 &= G_{12}(k_1 \mu_1 - 1), & t_5 &= G_2(1 - k_2 \mu_2) \\ t_3 &= \frac{-(1 + v_{23}) v_{21} E_1 + (1 - v_{21} v_{12}) E_2 m_1 \beta_1}{\Delta}, & \\ t_4 &= \frac{(1 + v_{23}) v_{21} E_1 k_1 + (1 - v_{21} v_{12}) E_2 \beta_1}{\Delta}, & \\ t_6 &= \lambda_2 k_2 + \lambda_2 \mu_2 + 2G_2 \mu_2, & \\ t_7 &= G_2(k_2 \mu_2 - 1), & t_8 &= -G_3(k_3 \mu_3 - 1) \end{aligned} \quad (21)$$

where $h_1 = \alpha D/2$ and $h_2 = \alpha t/2$.

3 Finite Element Analysis

In the analytical model for the analysis to determine the onset of buckling of fiber, the matrix is assumed to be infinitely thick. Without loss of generality and considering not to use an excessively long computational time for the finite element analysis, the matrix

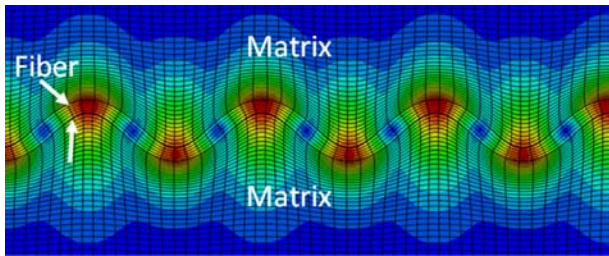


Fig. 6 Antisymmetric buckling mode obtained from linear buckling analysis in finite element analysis

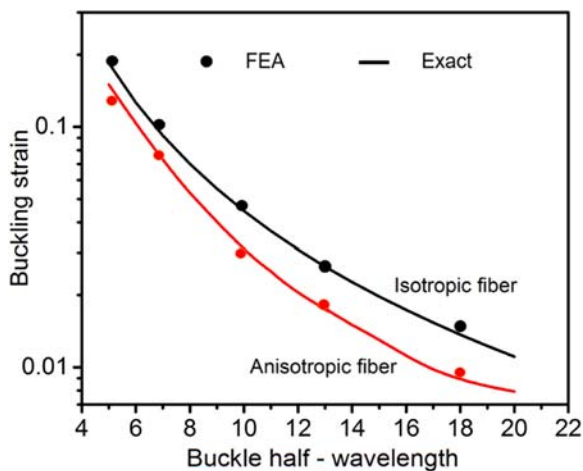


Fig. 7 Comparison of the buckling strain in logarithmic scale for the unidirectional composite for two situations where the carbon fiber is modeled as an anisotropic or as an isotropic material. In both anisotropic and isotropic models, the carbon fiber longitudinal modulus is set equal. It is seen that assuming isotropic behavior for a carbon fiber over-estimates the critical strain at buckling.

thickness is set to 50 times of the thickness of the fiber, and a periodic boundary condition is used at the two vertical edges. The analysis is conducted on ABAQUS 6.14 to compare with the theoretical results for the critical strain and buckling behavior. The fiber is modeled as a transversely isotropic linearly elastic material and the following parameters are used [44]: $E_{fx_1} = 276$ GPa, $E_{fy_1} = 19.5$ GPa, $G_{x_1y_1} = 70$ GPa, $v_{x_1y_1} = 0.28$, and $v_{y_1z_1} = 0.7$. The interphase region and the matrix are modeled as an isotropic, linearly elastic, and homogeneous material. The properties at the interphase region are considered to change with the volume fraction of the CNT sheet in the matrix, the Young's modulus in the interphase region increases as the volume fraction of the CNT sheet increases. The Poisson's ratio changes with CNT volume fraction as well [45]. An eight-node quadratic plane strain element is used for the fiber, interphase region and matrix. There are 1000 elements along the fiber direction, resulting in very small characteristic element lengths compared with the buckling wavelength. The total number of elements used is 50,000. In order to ensure the accuracy of the buckling strain, there are more than three elements along the thickness direction of the fiber and interphase region, and a mesh convergence study was conducted to ensure that mesh independence was achieved. The antisymmetric buckling modes observed from the finite element analysis are shown in Fig. 6, providing verification for assumption of antisymmetric buckling models assumed in the theoretical model development.

4 Results and Discussion

Parametric analysis was conducted using both the analytical model and FEA to examine the role of the thickness of the interphase region on the mechanical properties, and compressive strain at the onset of buckling. In Figs. 7–10, the solid lines represent theoretical results, and the symbols represent FEA simulation results. It is observed that the buckling strains versus buckle half-wavelength ($0.5 \lambda_w/D$) curves of modeling fiber as anisotropic or isotropic are quite different, as shown in Fig. 7. It is seen that for a fixed buckle half-wavelength, the buckling strain determined by modeling the fiber as anisotropic is significantly lower than that determined by modeling fiber as isotropic due to considering the lower transversely shear modulus. Figure 7 shows that the ratio of the isotropic model to anisotropic model buckling strain reaches a maximum difference of 57.5% at buckle half-wavelength 16, and Kardomateas and Simitses [46] observed that critical load from finite elements were as much as almost one-fifth with Euler load being for graphite/epoxy sandwich construction. The parameters used to determine the buckling strain and buckle half-wavelength are as follows:

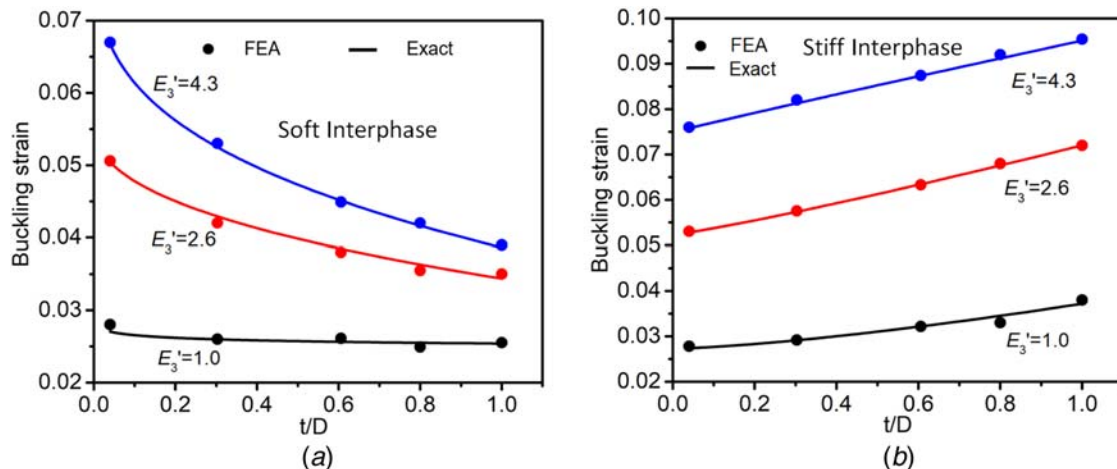


Fig. 8 Simulations and theoretical analysis are carried on at the same situation for both cases: (a) the buckling strain versus t/D for "soft" interphase region ($E_i < E_m$) and (b) the buckling strain versus t/D for "stiff" interphase region ($E_i > E_m$). Here, $E_{m0} = 3.5$ GPa and $E_3' = E_m/E_{m0}$.

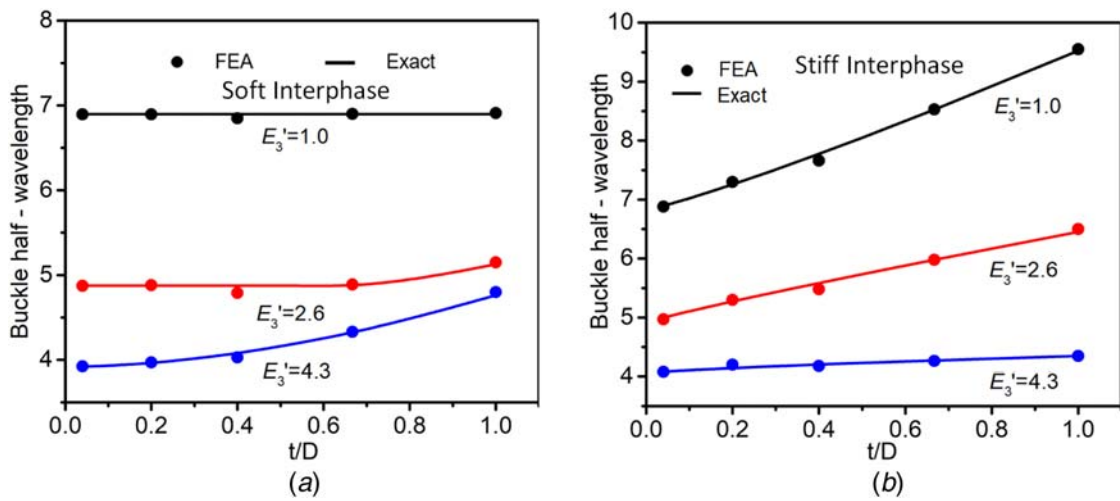


Fig. 9 Simulation and theoretical analysis are carried on at the same situation for both cases: (a) the buckle half-wavelength versus t/D for “soft” interphase region ($E_i < E_m$) and (b) the buckle half-wavelength versus t/D for “stiff” interphase region ($E_i > E_m$). Here $E_{m0} = 3.5$ GPa and $E_3 = E_{ir}/E_{m0}$.

Young's modulus of the matrix E_m is 3.5 GPa, Poisson's ratio of the matrix ν_m is 0.38, Young's modulus of the interphase region E_i is 20 GPa, Poisson's ratio of the interphase region ν_i is 0.33, and $t/D = 0.07$.

The effect of the interphase thickness was studied by changing the ratio of the interphase thickness to the fiber diameter. The result comparison is shown in Figs. 8(a) and 8(b). An excellent agreement has been reached between FEA results and the theoretical solution on the buckling strain, providing verification of the theoretical buckling analysis for a composite with a transversely isotropic fiber embedded in a surrounding nanocomposite interphase region and outer matrix. In FEA simulations, the maximum ratio of the interphase thickness to the fiber diameter is set at 1, the fiber diameter $D = 5 \mu\text{m}$ is fixed. In Fig. 8(a), when the ratio t/D increases, the buckling strain decreases in the case where the interphase region modulus 2.5 GPa is less than the matrix modulus, in a situation of a “soft” interphase region. The result indicates that a “soft” interphase region does not provide sufficient support for the carbon fibers under compression, making it prone to buckle. It is noted that the buckling strain increases with the increase of matrix modulus in Fig. 8(a). A stiffer lateral support it provides makes the carbon fiber more resilient to buckling under

compression. However, a reversed trend is observed in the case where the interphase region modulus is 25 GPa, larger than the matrix modulus, in a situation of (“stiff” interphase region in Fig. 8(b)). Figure 8(b) shows that wrapping CNTs on single carbon fiber increase the buckling strain, which increase linearly with the interphase thickness. The buckling strain increases by 35.9%, 36.3%, and 25.5% when the interphase thickness equals the fiber diameter for $E_3' = 1.0$, $E_3' = 2.6$, and $E_3' = 4.3$, respectively, in comparison with the baseline data when the fiber is surrounded by neat matrix. The higher matrix Young's modulus can help improve the buckling strain regardless of the interphase region property, both as shown in Figs. 8(a) and 8(b). It is seen that a thicker interphase region (a larger t/D) induces a larger wavelength for the “soft” and “stiff” interphase region in Figs. 9(a) and 9(b), to allow the buckle half-wavelength to decrease as the Young's modulus in the matrix increases. Figure 10 shows the results for the buckling strain as a function of the ratio of the interphase region modulus to matrix modulus from both theoretical analysis and FEA simulations. It is seen that E_i/E_m almost does not affect the buckling strain when the interphase thickness is very small. When the interphase thickness is comparable with the fiber diameter, the buckling strain increases with interphase Young's modulus initially, and it does not change much subsequently. There is an optimal Young's modulus in the interphase region around 17.5 GPa for such a composite since the buckling strain difference is only 1% for the interphase region modulus 17.5 GPa and 38.5 GPa, the last point in the graph, which can be achieved by controlling the volume fraction of CNTs and epoxy and the CNT sheet wrapping bias angle.

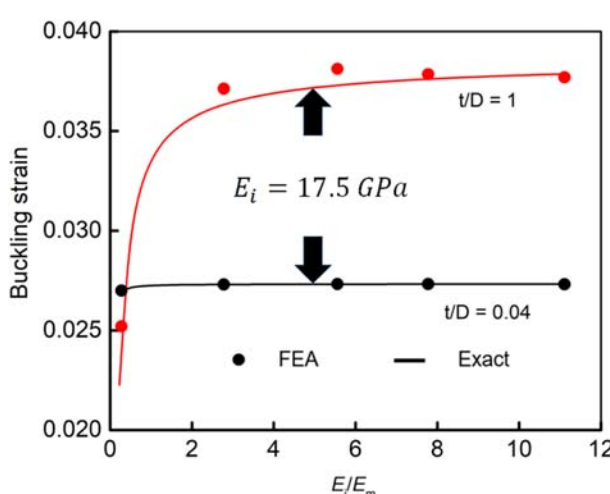


Fig. 10 The buckling strain versus Young's modulus ratio of the interphase region to the matrix. The dark arrows indicate the modulus of 17.5 GPa at the interphase region.

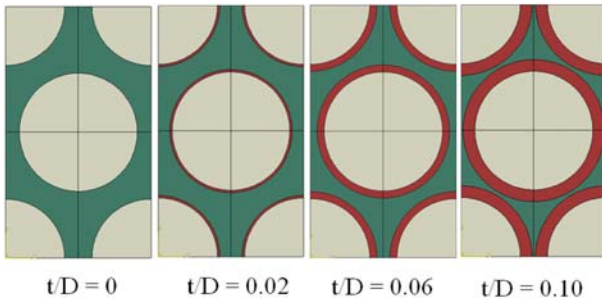


Fig. 11 Representative volume elements for different t/D ratios

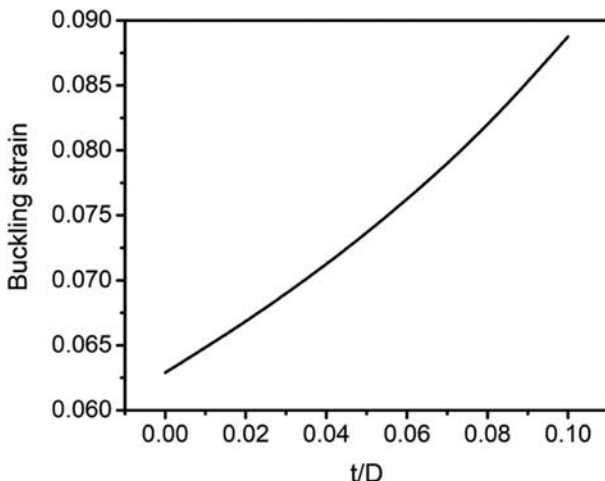


Fig. 12 Variation of the buckling strain as a function of the ratio of the interphase thickness to the fiber diameter for high fiber volume fraction in a unidirectional composite

ratios of t/D . To achieve this, the volume fraction of the matrix decreases as t/D increases as shown in Fig. 11. Simulations are carried out for the case of “stiff” interphase region where $E_i = 25$ GPa, $E_m = 15$ GPa, and the mechanical properties of fiber remained the same. As shown in Fig. 12, the buckling strain increases as the thickness of carbon nanotube sheet thickness increases when the carbon fiber volume fraction is high, which is consistent with the previous results for low fiber volume fraction. Compared with the buckling strain for carbon fiber composite ($t/D = 0$), the buckling strain of carbon nanotube sheet wrapped carbon fiber composite increases by 41.1% when $t/D = 0.1$. In comparison, the buckling strain improves only by 2.8% for dilute fibers when fiber volume fraction is low at the same t/D ratio. Hence, the buckling strain improves more when the carbon fiber volume fraction is high. In conclusion, adding CNT nanocomposite layer between carbon fiber and matrix improves significantly the buckling strain when the fiber volume fraction is high.

6 Summary and Conclusions

A theoretical model for studying the compressive buckling strain of a unidirectional carbon-fiber/epoxy composite was presented. In the model, the composite is considered to consist of three constituents: fiber, nanocomposite (CNT/matrix interphase region), and matrix. The fiber, nanocomposite, and matrix (e.g., epoxy) are modeled as a transversely isotropic and isotropic elastic continuum, respectively. The analysis is conducted under a plane strain condition applying a small perturbation in the field equations. Perfect bonding is assumed at the fiber/nanocomposite interface and nanocomposite/matrix interface to make sure displacement and traction are continuous at the interface. Buckling strain and corresponding

wavelength for antisymmetric deformation mode are obtained from the analysis. Finally, comparing the buckling strain determined by modeling fiber as anisotropic with modeling fiber as isotropic, the current model predicts lower buckling strain. FEA simulations were carried out to simulate the same buckling problem for model verification, and they show consistent results with the theoretical analysis. The effects of the nanocomposite thickness, Young’s modulus of the interphase region, and matrix on the buckling strain and wavelengths were discussed. Wrapping CNT sheet on carbon fiber is shown to help improve the compressive strength as long as Young’s modulus in the nanocomposite interphase region is higher than the matrix, which is readily achievable by controlling the volume fraction of CNT and the wrapping bias angle. The optimum interphase region thickness is equal to the fiber diameter under the assumption that the property of the fiber dominates the properties of composites for low fiber volume fraction. When the fiber volume fraction is high, such as 60% a value around a typical high-strength composite, adding nanocomposite between fiber and matrix has a more significant effect on improving compressive strength. These observations are further corroborated by molecular dynamics simulations reported elsewhere [47].

In summary, the theoretical analysis provides an effective tool for designing interphase in a composite through analysis of the compressive behavior of the composite with the consideration of the transversely isotropic fibers, and the analysis indicates that adding nanocomposite between fiber and matrix can improve significantly the compressive strength even when the fiber volume fraction is large.

Acknowledgment

We acknowledge the support of NSF (Funder ID: 10.13039/100003187) CMMI-1636306, CMMI-1661246, CMMI-1726435 and AFOSR FA9550-14-1-0227. Lu also thanks Louis A. Beecherl Chair for additional support, and Zhang acknowledges the support of the Eugene McDermott Graduate Fellowship.

Nomenclature

t	= thickness of the CNT/polymer matrix interphase region
D	= diameter of a fiber
E_i	= Young’s modulus in the i direction and $i \in \{1, 2, 3\}$
G_{ij}	= shear modulus in the $i-j$ plane, $i, j \in \{1, 2, 3\}$ and $i \neq j$
x, y, z	= Cartesian coordinates for the fiber, interphase region, and matrix
u, v, w	= displacements in the x, y , and z directions, respectively
CNTs	= carbon nanotubes
IFSS	= interfacial shear strength
FEA	= finite element analysis
x_i, y_i, z_i	= Cartesian coordinates for the fiber, interphase region, and matrix for $i = 1, 2, 3$, respectively
u_i, v_i, w_i	= displacements in the fiber, interphase region, and matrix for $i = 1, 2, 3$, respectively
$\Delta f_x, \Delta f_y$	= traction components in the x and y directions
Δf_z	= traction components in the z -direction
ϵ_{ij}	= strain components
κ, θ, μ	= direction cosines of the normal to the boundary element
σ_{ij}	= stress components
ν_{ij}	= Poisson’s ratio in the $i-j$ plane
λ	= Lamé constant
λ_w	= buckling wavelength

References

- [1] Liu, Z., Fang, S., Moura, F., Ding, J., Jiang, N., Di, J., Zhang, M., Lepró, X., Galvão, D., Haines, C., Yuan, N. Y., Yin, S. G., Lee, D. W., Wang, R., Wang, H. Y., Lv, W., Dong, C., Zhang, R. C., Chen, M. J., Yin, Q., Chong, Y. T., Zhang, R., Wang, X., Lima, M. D., Ovalle-Robles, R., Qian, D., Lu, H., and Baughman, R. H., 2015, “Hierarchically Buckled Sheath-Core Fibers for

- Superelastic Electronics, Sensors, and Muscles," *Science*, **349**(6246), pp. 400–404.
- [2] Mu, J., Hou, C., Wang, G., Wang, X., Zhang, Q., Li, Y., Wang, H., and Zhu, M., 2016, "An Elastic Transparent Conductor Based on Hierarchically Wrinkled Reduced Graphene Oxide for Artificial Muscles and Sensors," *Adv. Mater.*, **28**(43), pp. 9491–9497.
- [3] Tang, L.-G., and Kardos, J. L., 1997, "A Review of Methods for Improving the Interfacial Adhesion Between Carbon Fiber and Polymer Matrix," *Polym. Compos.*, **18**(1), pp. 100–113.
- [4] Williams, J. C., and Starke, E. A., Jr., 2003, "Progress in Structural Materials for Aerospace Systems," *Acta. Mater.*, **51**(19), pp. 5775–5799.
- [5] Soutis, C., 2005, "Carbon Fiber Reinforced Plastics in Aircraft Construction," *Mater. Sci. Eng. A*, **412**(1–2), pp. 171–176.
- [6] Hahn, H., and Sohi, M., 1986, "Buckling of a Fiber Bundle Embedded in Epoxy," *Compos. Sci. Technol.*, **27**(1), pp. 25–41.
- [7] Steif, P. S., 1987, "An Exact Two-dimensional Approach to Fiber Micro-Buckling," *Int. J. Solids Struct.*, **23**(9), pp. 1235–1246.
- [8] Tadjbakhsh, I. G., and Wang, Y., 1992, "Fiber Buckling in Three-Dimensional Periodic-Array Composites," *Int. J. Solids Struct.*, **29**(24), pp. 3169–3183.
- [9] Schultheisz, C. R., and Waas, A. M., 1996, "Compressive Failure of Composites, Part I: Testing and Micromechanical Theories," *Prog. Aerosp. Sci.*, **32**(1), pp. 1–42.
- [10] Waas, A. M., and Schultheisz, C. R., 1996, "Compressive Failure of Composites, Part II: Experimental Studies," *Prog. Aerosp. Sci.*, **32**(1), pp. 43–78.
- [11] Kyriakides, S., Arsecularatne, R., Perry, E., and Liechti, K., 1995, "On the Compressive Failure of Fiber Reinforced Composites," *Int. J. Solids Struct.*, **32**(6–7), pp. 689–738.
- [12] Yongbo, Z., and Huimin, F., 2011, "On the Longitudinal Compressive Strength Prediction of Unidirectional Laminated Composites Based on An Improved Model," *Polym. Compos.*, **32**(11), pp. 1817–1826.
- [13] Harich, J., Lapusta, Y., and Wagner, W., 2009, "3d FE-Modeling of Surface and Anisotropy Effects During Micro-Buckling in Fiber Composites," *Compos. Struct.*, **89**(4), pp. 551–555.
- [14] Ji, W., and Waas, A. M., 2007, "Global and Local Buckling of a Sandwich Beam," *J. Eng. Mech.*, **133**(2), pp. 230–237.
- [15] Waas, A., Babcock, C., and Knauss, W., 1990, "A Mechanical Model for Elastic Fiber Microbuckling," *ASME J. Appl. Mech.*, **57**(1), pp. 138–149.
- [16] Rosen, B. W., 1965, "Mechanics of Composite Strengthening," *NASA Technical Reports*, American Society for Metals, Materials Park, OH, pp. 37–75.
- [17] Greszczuk, L., 1975, "Microbuckling Failure of Circular Fiber-Reinforced Composites," *AIAA J.*, **13**(10), pp. 1311–1318.
- [18] Lo, K., and Chim, E.-M., 1992, "Compressive Strength of Unidirectional Composites," *J. Reinf. Plast. Compos.*, **11**(8), pp. 838–896.
- [19] Yeh, J., and Teply, J., 1988, "Compressive Response of Kevlar/epoxy Composites," *J. Compos. Mater.*, **22**(3), pp. 245–257.
- [20] Xu, Y. L., and Reifsnider, K. L., 1993, "Micromechanical Modeling of Composite Compressive Strength," *J. Compos. Mater.*, **27**(6), pp. 572–588.
- [21] Zhang, G., and Latour, R. A., Jr., 1994, "An Analytical and Numerical Study of Fiber Microbuckling," *Compos. Sci. Technol.*, **51**(1), pp. 95–109.
- [22] Lapusta, Y., Harich, J., and Wagner, W., 2008, "Three-Dimensional FE Model for Fiber Interaction Effects During Microbuckling in Composites With Isotropic and Anisotropic Fibers," *Int. J. Numer. Methods Biomed. Eng.*, **24**(12), pp. 2206–2215.
- [23] Bai, Z., Su, Y., and Ji, B., 2016, "Buckling Behaviors of Staggered Nanostructure of Biological Materials," *ASME J. Appl. Mech.*, **83**(3), p. 031011.
- [24] Su, Y., Ji, B., Hwang, K.-C., and Huang, Y., 2012, "Micro-Buckling in the Nanocomposite Structure of Biological Materials," *J. Mech. Phys. Solids*, **60**(10), pp. 1771–1790.
- [25] Parnes, R., and Chiskis, A., 2002, "Buckling of Nano-Fibre Reinforced Composites: A Re-examination of Elastic Buckling," *J. Mech. Phys. Solids*, **50**(4), pp. 855–879.
- [26] Lapusta, Y., Labesse-Jied, F., Samborskaya, A., and Wagner, W., 2011, "On the Effects of Interacting Anisotropic Fibers on the Microbuckling in a Composite," *Int. J. Fract.*, **167**(1), pp. 103–110.
- [27] Andrianov, I. V., Kalamkarov, A. L., and Weichert, D., 2012, "Buckling of Fibers in Fiber-Reinforced Composites," *Compos. Part B: Eng.*, **43**(4), pp. 2058–2062.
- [28] Luo, H., Roy, S., and Lu, H., 2012, "Dynamic Compressive Behavior of Unidirectional Im7/5250-4 Laminate After Thermal Oxidation," *Compos. Sci. Technol.*, **72**(2), pp. 159–166.
- [29] Maurin, R., Davies, P., Baral, N., and Baley, C., 2008, "Transverse Properties of Carbon Fibres by Nano-Indentation and Micro-Mechanics," *Appl. Compos. Mater.*, **15**(2), pp. 61–73.
- [30] Miyagawa, H., Sato, C., Mase, T., Drown, E., Drzal, L. T., and Ikegami, K., 2005, "Transverse Elastic Modulus of Carbon Fibers Measured by Raman Spectroscopy," *Mater. Sci. Eng. A*, **412**(1–2), pp. 88–92.
- [31] Roy, S., Lu, H., Narasimhan, K., and Hussain, F., 2005, "Characterization and Modeling of Strength Enhancement Mechanisms in a Polymer/Clay Nanocomposite," 46th AIAA/ASME/ASCE/AHS/ASC Structures, Structural Dynamics and Materials Conference, Austin, TX, Apr. 18–21. American Institute of Aeronautics and Astronautics, p. 1853.
- [32] Roy, S., Hussain, F., Narasimhan, K., Vengadasalam, K., and Lu, H., 2007, "E-glass/Polypropylene Pultruded Nanocomposite: Manufacture, Characterisation, Thermal and Mechanical Properties," *Polym. Polym. Compos.*, **15**(2), pp. 91–102.
- [33] Waas, A., 1992, "Effect of Interphase on Compressive Strength of Unidirectional Composites," *ASME Trans. Ser. E J. Appl. Mech.*, **59**, pp. S183–S188.
- [34] Maligno, A., Warrior, N., and Long, A., 2010, "Effects of Interphase Material Properties in Unidirectional Fibre Reinforced Composites," *Compos. Sci. Technol.*, **70**(1), pp. 36–44.
- [35] Drzal, L., 1990, "The Role of the Fiber-Matrix Interphase on Composite Properties," *Vacuum*, **41**(7–9), pp. 1615–1618.
- [36] Lane, R., Hayes, S., and Jones, F., 2001, "Fibre/matrix Stress Transfer Through a Discrete Interphase: 2. High Volume Fraction Systems," *Compos. Sci. Technol.*, **61**(4), pp. 565–578.
- [37] Zhang, F.-H., Wang, R.-G., He, X.-D., Wang, C., and Ren, L.-N., 2009, "Interfacial Shearing Strength and Reinforcing Mechanisms of An Epoxy Composite Reinforced Using a Carbon Nanotube/Carbon Fiber Hybrid," *J. Mater. Sci.*, **44**(13), pp. 3574–3577.
- [38] Lu, H., Baughman, R. H., Haque, M. H., and Fang, S. D., 2017, "Method of Fabricating Carbon Nanotube Sheet Scrolled Fiber Reinforced Polymer Composites and Compositions and Uses Thereof," US Patent No. 9,758,628.
- [39] Aliev, A. E., Oh, J., Kozlov, M. E., Kuznetsov, A. A., Fang, S., Fonseca, A. F., Ovalle, R., Lima, M. D., Haque, M. H., Gartstein, Y. N., Zhang, Mei, Zakhidov, Anvar A., and Baughman, Ray H., 2009, "Giant-stroke, Superelastic Carbon Nanotube Aerogel Muscles," *Science*, **323**(5921), pp. 1575–1578.
- [40] Huang, G., and Lu, H., 2006, "Measurement of Young's Relaxation Modulus Using Nanoindentation," *Mech. Time-Dependent Mater.*, **10**(3), pp. 229–243.
- [41] Briscoe, B., Fiori, L., and Pefillo, E., 1998, "Nano-Indentation of Polymeric Surfaces," *J. Phys. D: Appl. Phys.*, **31**(19), pp. 2395–2405.
- [42] Xu, T., Luo, H., Xu, Z., Hu, Z., Minary-Jolandan, M., Roy, S., and Lu, H., 2018, "Evaluation of the Effect of Thermal Oxidation and Moisture on the Interfacial Shear Strength of Unidirectional IM7/BMI Composite by Fiber Push-In Nanoindentation," *Exp. Mech.*, **58**(1), pp. 111–123.
- [43] Novozhilov, V. V., 1999, *Foundations of the Nonlinear Theory of Elasticity*, Courier Corporation, Mineola, New York.
- [44] Upadhyaya, P., Roy, S., Haque, M. H., and Lu, H., 2013, "Influence of Nano-Clay Compounding on Thermo-Oxidative Stability and Mechanical Properties of a Thermoset Polymer System," *Compos. Sci. Technol.*, **84**, pp. 8–14.
- [45] Tsuda, T., Ogasawara, T., Moon, S.-Y., Nakamoto, K., Takeda, N., Shimamura, Y., and Inoue, Y., 2014, "Three Dimensional Orientation Angle Distribution Counting and Calculation for the Mechanical Properties of Aligned Carbon Nanotube/epoxy Composites," *Compos. Part A: Appl. Sci. Manuf.*, **65**, pp. 1–9.
- [46] Kardomateas, G. A., and Simitses, G. J., 2004, "Comparative Studies on the Buckling of Isotropic, Orthotropic, and Sandwich Columns," *Mech. Adv. Mater. Struct.*, **11**(45), pp. 309–327.
- [47] Ravindranath, P. K., Roy, S., Unnikrishnan, V., Wang, X., Xu, T., Baughman, R., and Lu, H., 2019, "A Multiscale Model to Study the Enhancement in the Compressive Strength of Multi-Walled CNT Sheet Overwrapped Carbon Fiber Composites," *Compos. Struct.*, **219**, pp. 170–178.